PHYSICAL CONDITIONS AND CURRENT MASSIVE STAR FORMATION IN NGC 3603

M. Tapia,[1] J. Bohigas, and B. Pérez

Instituto de Astronomía, UNAM, Ensenada, México

M. Roth

Las Campanas Observatory, CIW, Chile

and

Ma. T. Ruiz[1]

Departamento de Astronomía, Universidad de Chile

RESUMEN

Se obtuvieron nuevas observaciones ópticas y en el infrarrojo de la región H II Galáctica NGC 3603, para explorar la interacción entre el cúmulo de formación estelar HD 97950 y el material restante de la nube molecular, así como la formación de nuevas generaciones de estrellas de tipo OB. Encontramos evidencia de que en los últimos tres a seis millones de años, se ha dado un proceso de formación estelar que ha ido avanzando ininterrumpidamente hacia el sur. Encontramos 50 objetos con exceso de emisión en la banda K. El 80% está en asociaciones o vinculado a otros síntomas de formación estelar. Varios están en las puntas de los frentes de ionización creados por HD 97950. Algunos son jóvenes estrellas OB con máseres de agua cercanos y/o asociados a picos de emisión en el radiocontinuo. Dentro de $15''$ centrado en Irs 9, hay 12 estrellas de tipo OB (de un total de 16) que presentan grandes excesos de emisión mas allá de 2 μm. La estrella más masiva de esta nueva generación estelar en NGC 3603 es de tipo O5–O6.

ABSTRACT

New optical and near-infrared observations of the Galactic H II region NGC 3603 have been obtained in order to explore the interaction of the central starburst cluster HD 97950 with the remains of the molecular cloud and the formation of new generations of OB-type stars. Ample evidence for continuous stellar formation activity proceeding from north to south over the past three to six million years is presented. K-band excesses are found in 50 objects which are the youngest OB-type stars in the region. Nearly 80% is clustered or associated to signposts of recent star formation. Several sources are found near the tips of the ionization fronts produced by HD 97950. Some of these are young OB stars with water masers in their vicinity and/or associated to isolated radio-continuum emission peaks. Near the centre of the active star formation region that is further away from HD 97950, the Irs 9 cluster, 12 OB-type stars (out of 16) with large excess emission beyond 2 μm are found within a $15''$ radius. The most massive star of this new stellar generation in NGC 3603 is an O5–O6 star.

Key Words: **H II REGIONS — ISM: NGC 3603 — STARS: FORMATION**

39

1. INTRODUCTION

The importance of NGC 3603, the most massive optically visible H II region in our Galaxy (Goss & Radhakrishnan 1969), has been widely stressed in recent years. It is powered by the Galactic prototype of a starburst cluster, which contains more than 50 WR-O3-B0 stars (Melnick, Tapia, & Terlevich 1989; hereafter MTT). At its nucleus, known as HD 97950, it has a stellar mass density of $\sim 10^5 \, M_\odot \, \mathrm{pc}^{-3}$. The stellar population of the starburst cluster has been studied in great detail by MTT, Drissen et al. (1995), Moffat, Drissen, & Shara (1994) and Hofmann, Seggewiss, & Weigelt (1995) at visible wavelegths, and by Eisenhauer et al. (1998) as well as Brandl et al. (1999) in the near-infrared. The distance to the star cluster, $d = 7.2$ kpc (MTT), is well established both photometrically and spectroscopically. Extinction across the nucleus of the cluster, which comprises most of the stars, is rather constant ($E_{B-V} = 1.44 \pm 0.13$, MTT) as practically all intracluster gas and dust has been swept away by the huge stellar winds, up the the boundaries of the well known "empty bubble" of approximately $30''$ radius (Balick, Boeshaar, & Gull 1980, MTT).

The mass function of the starburst cluster does not differ greatly from Salpeter's power law for massive stars (Moffat et al. 1994), while there may be evidence for a flatter power law for low-mass stars (Eisenhauer et al. 1998). There seems to be a discrepancy concerning the age of the starburst cluster: the most massive stars ($> 10 \, M_\odot$) have ages between 1 and 3 million years (MTT), but the age of lower mass stars seems to be between 0.3 and 1.0 million years (Eisenhauer et al. 1998; Brandl et al. 1999). This difference may be real, but notice that estimates for the age of low mass stars depend heavily on which pre-main sequence evolutionary model is used. Although based on a small number of stars, age stratification with a well defined pattern has been suggested by Tapia (1981a), Persi et al. (1985) and MTT. By comparing the predicted number of field stars per unit area brighter than a certain K magnitude limit in the direction of NGC 3603 calculated using Jones et al.'s (1981) Galactic model, Persei et al. (1985) showed that towards NGC 3603, there is an excess by a factor of more than 5 in the number of K-bright K-M stars. These were classified by Frogel, Persson, & Aaronson (1977, hereafter FPA) and Persi et al. (1985) as late-type supergiants at a distance similar to NGC 3603. This statistically significant number of evolved very massive stars is located a few arcminutes to the north and to the northeast of HD 97950, in a region which is now free of dense material (Persi

et al. 1985; Melnick 1989). On the other hand, several sites marked by the presence of very young objects are located to the south of HD 97950.

The characteristics of the ionized gas in NGC 3603 have been studied less extensively than its stellar content. Low resolution radio (line and continuum) measurements have been reported by Retallack & Goss (1980) and, at higher resolution, by DePree, Nysewander, & Goss (1999). Maps of the region in several infrared lines were presented by Lacy, Beck, & Geball (1982). A morphological study based on photographic plates and narrow-band filters, supplemented by a Fabry-Pérot kinematical study of several regions in the nebula, was made by Balick et al. (1980). Hα and [N II] HST images were presented by Brandner et al. (2000). Finally, a long slit optical spectrum of the nebula was reported by MTT.

The first indication of star formation activity in NGC 3603 was presented by FPA, who found extended and multi-peaked mid-infrared emission to the south and southwest of HD 97950, with a number of very red near-infrared sources associated with the region[2]. These were mapped and studied with more detail in the near-IR by Persi et al. (1985) and Roth et al. (1987). CO emission peaks were found near but not coincident with the mid-infrared peaks (Melnick 1989). Clearly, a new generation of stars is being formed as a result of the interaction between the stellar winds from HD 97950 and the remains of the molecular cloud.

In order to understand the details of these interactions and the properties of the youngest embedded objects, we present a detailed spectroscopic and morphological optical line-emission study of the entire H II region, supplemented with a near-infrared imaging photometric study of an area 245×245 sq arcsec centred $45''$ south of HD 97950. This area covers the known CO and mid-infrared emission peaks of the region. The observations are described in the next section, results are presented in § 3 with a discussion of the most conspicuous objects. The last section summarizes the new findings.

2. OBSERVATIONS

2.1. *Optical Imaging*

Images of the region were obtained at Las Campanas Observatory in March 18–21 1994, using the 1m telescope (LCO-40) and the TEK1 1024x1024 pixel detector. These images cover a field of view of

---

[2] The coordinates of the infrared sources in NGC 3603 given by Frogel et al. (1977) are systematically shifted in right ascension by -2.1^s.
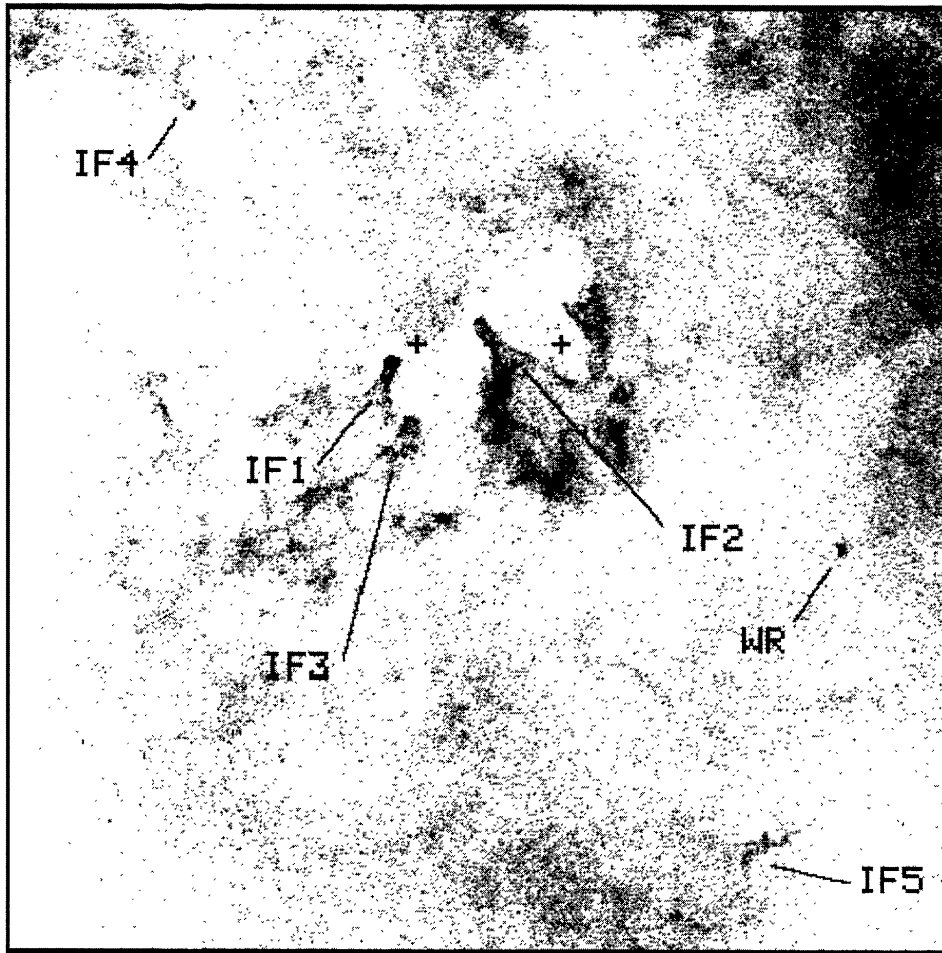
Fig. 1. Continuum-subtracted [S II] $\lambda 6724$ image covering 630×660 sq arcseconds. Ionization fronts mentioned in the text are marked (IF) and the nebula Wray 15–780 surrounding the Wolf-Rayet star MR 37 is also marked (WR). The plus signs mark the positions P1, P2, and P3 (from W to E) along the slit where the spectrum was extracted and measured. The centre of the image is at $\alpha = 11^h15^m03.7^s$; $\delta = -61°17'37''$ (2000.0). North is up, east to the left.

707×707 sq arcseconds and were obtained for the following emission lines (exposure time in parenthesis): Hβ (1800 s), Hα (600 s), [O III] $\lambda 5007$ (1500 s), [N II] $\lambda 6584$ (1500 s), [S II] $\lambda 6724$ (1800 s; both lines), and [S III] $\lambda 9069$ (600 s). Continuum images, each exposed for 300 s, were taken at the following wavelengths: 4772 Å, 5050 Å, 6650 Å, and 8950 Å. Plate scale is 0.69″/pixel, and the average FWHM of stellar images was ~ 2 pixel during the whole observing run. The San Pedro Mártir Series I set of nebular filters was used (their properties can be found at http://bufadora.astrosen.unam.mx/Instruments/filtros/filtros.html). Filters were designed for an f/7.5 converging beam, nearly the same as in LCO-

40, and an operating temperature of 0°C. Dome temperature during our observations was 13°C on average, which would shift the filter's transmission curve ~ 2.5 Å to the red. Since the minimum bandwidth of these filters is 11 Å, all the inspected lines fall within the transmission curves.

Continuum was subtracted matching the star counts of line and continuum images, as determined with the DAOPHOT IRAF[3] package. More than 50 stars were used for each pair of images (line and continuum).

_____

[3]IRAF is disributed by NOAO which is operated by AURA under contract to the NSF.
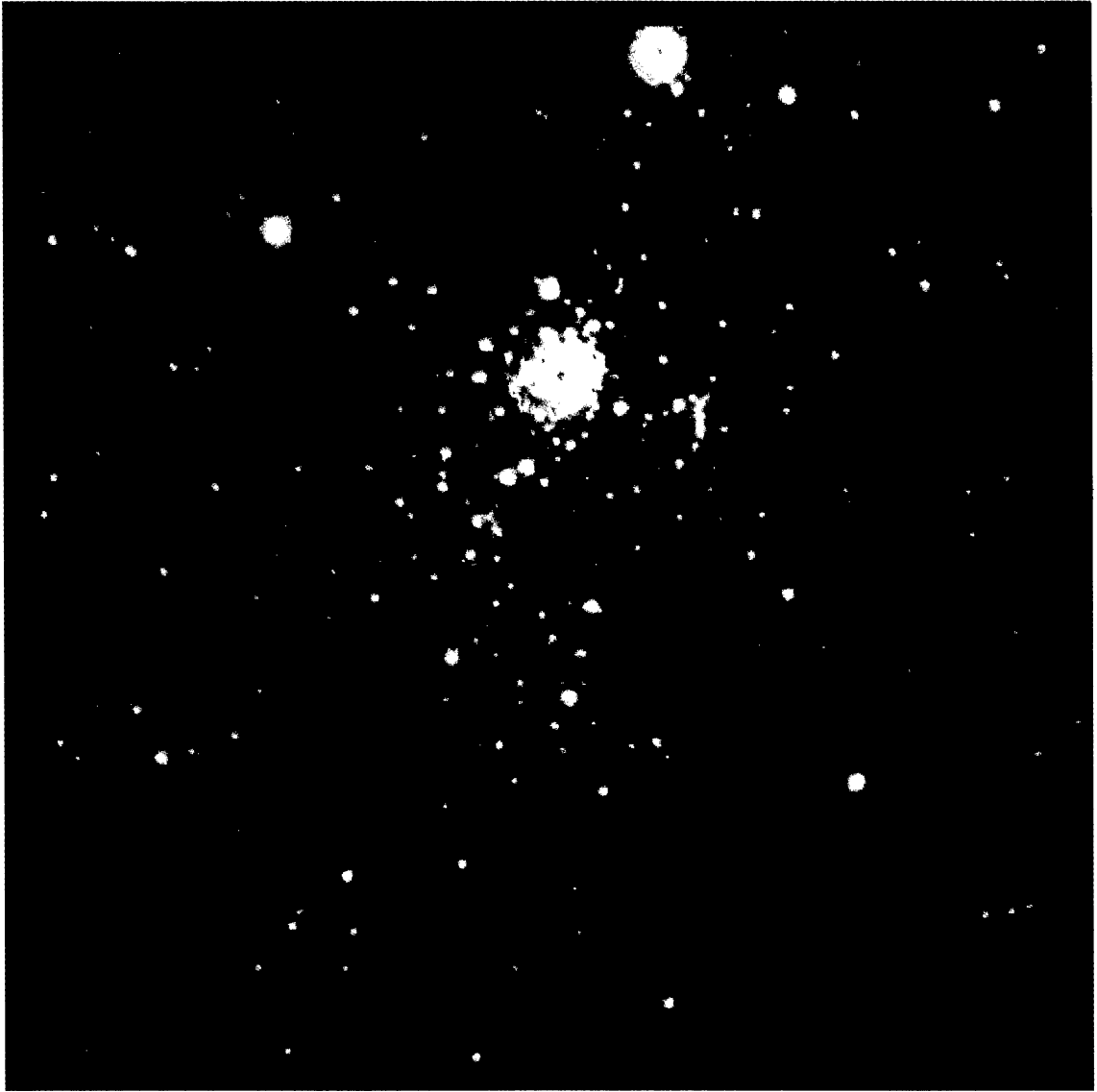
Fig. 2. Color composite image from the CTIO J, H, and K (*blue, green, and red*, respectively) mosaics of NGC 3603. The centre is at $\alpha = 11^h 15^m 08.6^s$, $\delta = -61° 16' 21''$ (2000.0) and the field of view is 240×240 sq arcseconds. North is up, east to the left.

2.2. *Spectroscopy*

Spectroscopy was carried out in May 30 1995, with the RC spectrograph, the 4 m telescope at CTIO and the Loral 3K chip. The spectral setup consisted of the KPGL#3 grating and a 175 μm wide slit (corresponding to 1.5″) aligned in the EW direction. The mean spectral resolution and dispersion are $\sim$ 3 pixel and 1.21 Å/pixel, respectively. The wavelength range covered is 3650–7300 Å. The exposure time was 240 seconds. Standard star LTT 3218 was used for flux calibration.

Data reduction was performed using IRAF standard procedures. Results are presented in Table 1. These are for a 1.5″ × 4.9″ aperture (NS and EW axes, respectively) at three positions, all of them referred to GSC 8959–01463 from the Hubble Guide Star Catalogue ($\alpha = 11^h 14^m 46.97^s$, $\delta = -61°15'59.9''$, equinox 2000.0): P1 (50″E,6″S), P2 (103″E,6″S) and P3 (154″E,6″S). Aperture centres, marked on Figure 1, are correct within $\sim$ 1.5″. Reddening corrections were made with Seaton's (1979) extinction law, assuming that Hα/Hβ = 2.85. Errors
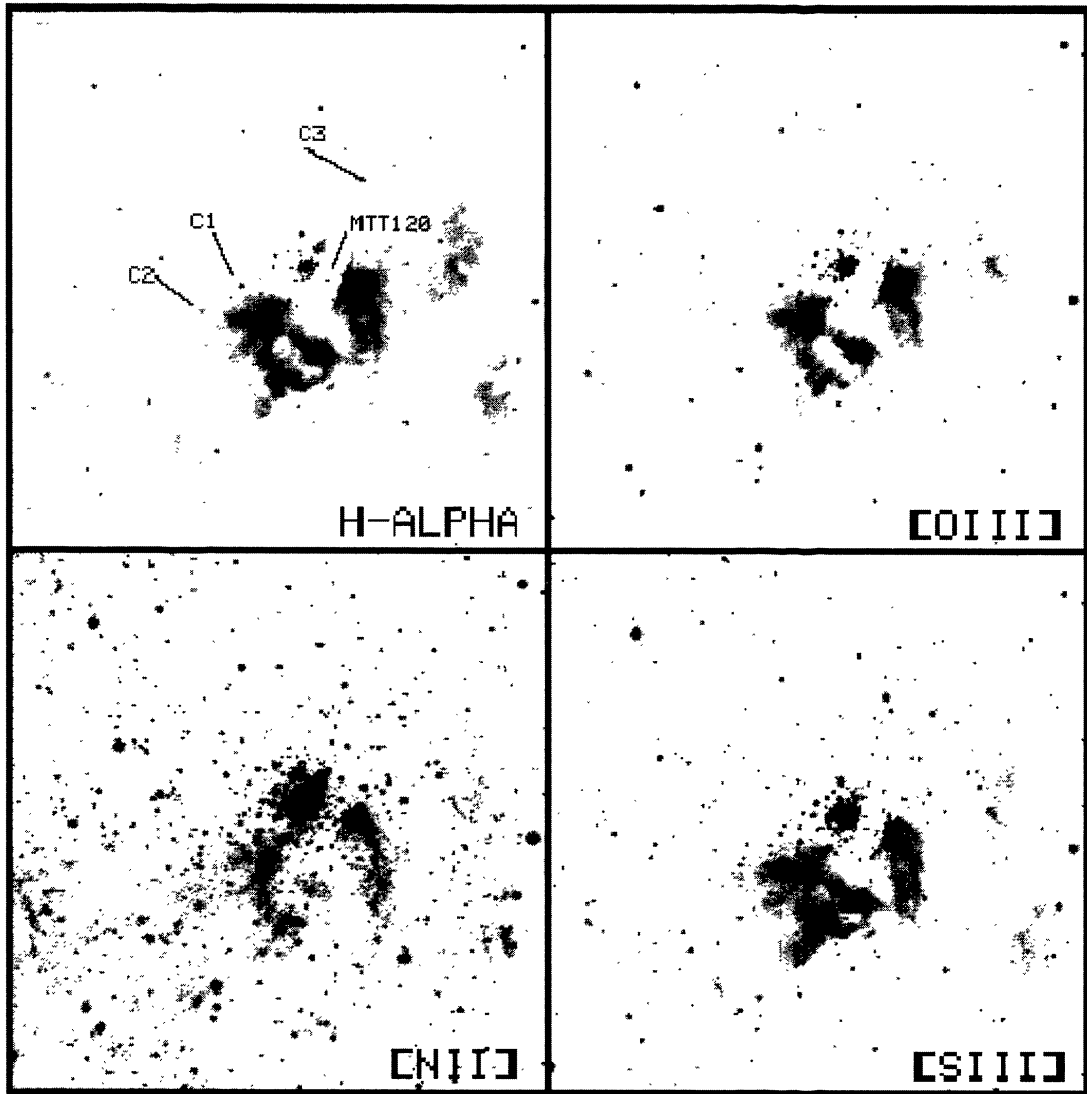
Fig. 3. Collage of the CCD narrow-band images taken in the Hα, [N II] λ6584, [O III] λ5007, and [S III] λ9069 atomic lines. C1, C2, and C3 mark the positions of Brandner et al.'s (2000) "proplyds" and MTT120 marks the emission line star #120 from Melnick, Tapia, & Terlevich (1989). The field of view is 170 × 170 sq arcseconds. North is up, east to the left.

smaller than 10% are expected for line fluxes larger than $\sim 10^{-14}$ erg cm^{-2} s^{-1}. Uncertainties can be as large as 20% for the smallest fluxes reported in Table 1 ($\sim 10^{-15}$ erg cm^{-2} s^{-1}, some 20 times less than the Hβ flux at position P2).

2.3. Near-Infrared Imaging

Two sets of mosaics of NGC 3603 in the JHK bands were constructed. An area of 70 × 70 sq arcsec centred on HD 97950 was imaged with the IR camera (Persson et al. 1992) attached to the 2.5 m DuPont telescope at Las Campanas Observatory in November 1993. The image scale is 0.35″ per pixel and the mean point-spread function (FWHM) less than 0.9″. The total exposure time was 80 s for each of the JHK frames.

A larger region (260 × 260 sq arcsec), centred some 45″south of HD 97950, was imaged and mosaiced using a similar set of filters with OSIRIS mounted on the 1.5 m telescope at Cerro Tololo In-

teramerican Observatory. In the imaging mode of this telescope, OSIRIS yields a scale of 0.49″/pixel. The total integration time with each filter was also 80 s and the measured point-spread function (FWHM) is 1.2″.

Each frame was sky-subtracted, flat-fielded and averaged following the normal procedure. Figure 2 shows the composite JHK "true color" image from the CTIO frames. Photometry was performed with DAOPHOT (ALLSTAR) under IRAF (Stetson 1987). Photometric calibrations were obtained for both sets, observing several standard stars with the same airmass range covered during the exposures on NGC 3603. Non-linearity effects of the CTIO camera were corrected matching the photometry of the common set of stars. These corrections also improve the match between photometries taken through the slightly different sets of JHK filters. Completeness limits are around 14.3 in all filters. The estimated largest photometric errors are 0.14 and 0.20 for the LCO and CTIO observations.

We detected 548 sources in the K band, 373 of which were measured in the three bands. For stars in common, preference was given to the LCO photometry. Astrometry was performed using a grid of stars from the HST Guide Star Catalogue and several visible stars in our field. The infrared measured positions are accurate to 1″. When comparing our coordinates with those given by FPA for seven sources in common, we found that the latter are systematically shifted -2.1^s in right ascension.

3. RESULTS AND DISCUSSION

3.1. *Spectroscopy*

Temperatures could not be measured since [O III] 4363 and [N II] 5755 were not detected. The electron density was determined from the [S II] $\lambda6717$/[S II] $\lambda6731$ line ratio using the *nebular* package from the Space Telescope Science Data Analysis System. The S$^+$ lines are weak but well defined in the three inspected regions, and ratios are probably precise at the $\sim 5\%$ level. The densities derived from this ratio, assuming that $T_e = 9000$ K, are 120^{+65}_{-55} (P1), 690^{+150}_{-130} (P2) and 90^{+70}_{-60} (P3) cm^{-3}. Ion concentrations at position P2, the only one for which we have information on such important ions as O$^+$, Ne^{+2}, and S^{+2}, are given in Table 2. We assume that the electron temperature is uniform and equal to 9000 K. Upper and lower bounds for ion concentrations and chemical abundances are for $T_e = 8000$ K (upper bounds for all ions except helium) and $T_e = 10,000$ K (lower bounds for all ions except helium). The abundance of He$^+$ was deter-
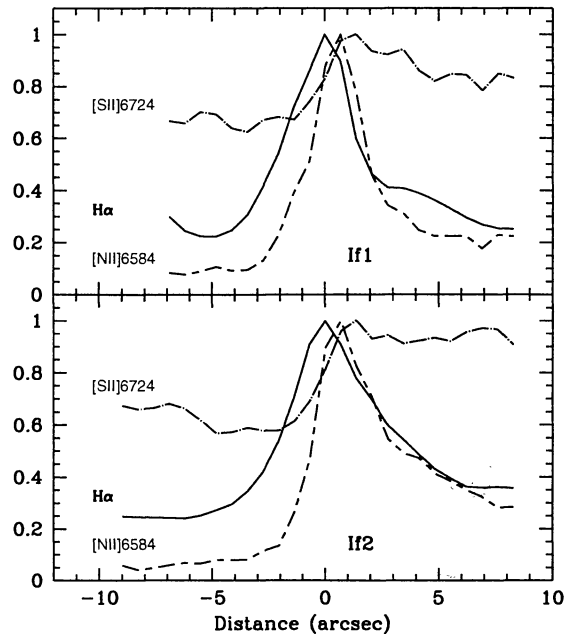

Fig. 4. Normalized intensity profiles of Hα, [N II], and [S II] accross ionization fronts If1 and If2. The position angles for these cuts are 337° (If1) and 55° (If2).

mined following Aller (1984). All other ion abundances were determined with the *nebular* package from the Space Telescope Science Data Analysis System. Elemental abundances, also shown in Table 2, were calculated with the standard ionization correction factors (equations A1, A28, A30, and A36 in Kingsburg & Barlow 1994).

Spectroscopic observations at an unspecified position were reported by MTT. We recalculated the physical conditions with their spectral data and found that their inspected region has a slightly higher temperature than assumed here (9800 K), but is much denser (4850 cm^{-3}). The abundances of oxygen and neon derived from our spectral data are 1.3 and 2 times larger if $T_e = 9000$ K, but are nearly identical if $T_e = 10,000$ K. We find the nitrogen abundance to be significatively smaller with the assumed temperature range. These discrepancies may arise for a number of reasons, above all from the use of a single temperature model.

3.2. *Optical Imaging*

Narrow-band images of the central region of NGC 3603 in the light of Hα, [N II] $\lambda6584$, [O III] $\lambda5007$, and [S III] $\lambda9069$ are shown in Figure 3. Some localized features are labeled in the

Fig. 5. Color composites of the continuum-subtracted narrow-band CCD images of NGC 3603 revealing the ionization structure. Upper panel: [O III] λ5007 (*blue*), Hα (*green*), and [S III] λ9069 (*red*). The centre is at $\alpha = 11^h15^m02.2^s$; $\delta = -61°15'40''$ (2000.0), and the field of view is 500×375 sq arcseconds. Lower panel: [O III] λ5007 (*blue*), [N II] λ6584 (*green*), and [S II] λ6724 (*red*). The centre is at $\alpha = 11^h15^m04.1^s$; $\delta = -61°15'35''$ (2000.0). The bright spot close to the lower-right corner is the wind-blown nebula Wray 15–780 associated with WR CSI-61-11124 = MR 37. North is up, east to the left.
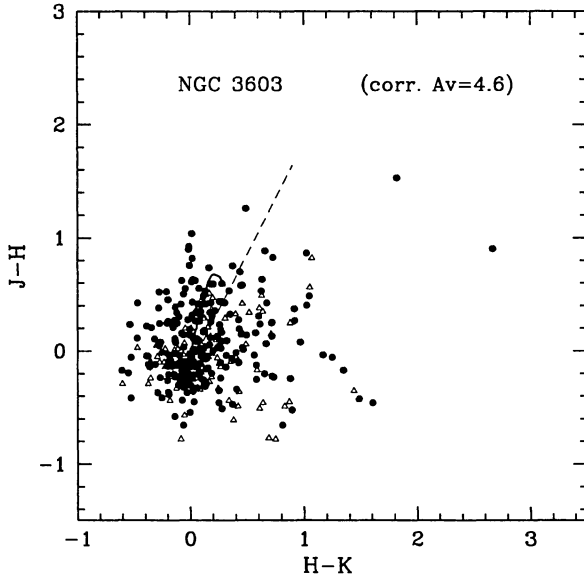
Fig. 7. $H - K$ versus $J - H$ diagram for sources measured in J, H, and K. Open triangles are stars located within the starburst cluster. The solid line represents the position of main sequence stars and the broken line, the reddening vector.

them is substantially above the mean. On the other hand, Hα/[S II] λ6724 is close to a factor of 2 larger in the condensations than in the immediate environment. This indicates that there is less neutral material within them, and suggests that an **additional** ionizing source lies within the condensations. On the basis of a red continuum excess in the optical spectrum of region C1 (their region C13), Dottori et al. (1999) also argue that there may be an embedded source, a contention supported by our near-infrared images, which show K-band excess emission in this region (and not in C2). The condensations also stand out in the Hα/[N II] ratio which is some 2 times smaller within them, but are not obvious in the Hα/[O III] and Hα/[S III] frames. No other condensation with similar morphological and spectral features was found in our whole field of view (707×707 sq arcseconds).

An [O III] λ5007/Hα image (continuum subtracted but not corrected for reddening) of the central part of NGC 3603 is shown in Figure 6. A few narrow "lanes" where this ratio is comparatively smaller delineate the edges of ionization fronts If1 and If2. These prominent "lanes" disappear

when the image is dereddened, i.e., these "lanes" are characterized by a higher than average extinction rather than lower than average excitation. Similar structures may also become less prominent after extinction corrections are applied. Not so with the most remarkable structure in this line ratio image, a comparatively more highly excited (higher value of [O III] λ5007/Hα) semicircular arc (marked in Fig. 6) centred at C1 and extending some 3″ to the north. This arc is not apparent in either one of the source frames but only on the ratio image. The concave side of the arc is in the general direction of HD 97950, and it probably is an ionization front moving into the C1 condensation. The size of the arc (side to side) is around 3″, or 0.1 pc at the distance of NGC 3603. In comparison with classical "proplyds" (e.g., Orion) this structure is extremely large. It should not be confused with the faint and much more extended filaments around condensation C1 that Brandner et al. (2000) identify as bow shocks. These filaments appear in our Hα and [O III] λ5007 images, but not in the [N II] λ6584 and [S II] λ6724 frames, which implies that photoionization, rather than shock waves, is the most likely excitation mechanism.

Surprisingly, there was only one previously unknown emission line star evidenced by our continuum-subtracted Hα frame. This star is listed 120 by MTT and is located 15″ to the SW of HD 97950. It presents a considerable 2.2 μm excess emission (Table 3) and will be discussed in § 3.3.

We also report the detection of the small ($\sim$ 12″ diameter) lopsided (to the NE) emission nebula Wray 15–780 (labeled WR in Fig. 1) associated to the WR star MR 37 = CSI-61-11124 (α = 11^{h}14^{m}28.5^s, δ = $-$61°18′22″, epoch = 2000.0). The star was listed in Morton Robert's (1962) catalogue of Wolf-Rayet stars. It was later discarded by Smith (1968) on grounds of the absence of emission lines characteristic of the WR phenomenon from this star in her blue objective-prism survey, but this may be explained by the fact that the star is very highly reddened. Henize (1976) found moderately weak, widened Hα emission over a faint red continuum. It is a radio-continuum source (te Lintel Hekkert et al. 1991) and an IRAS point source, implying the presence of ionized material close to the star and dust particles further away from it. Its visible and near-infrared colors (V = 11.5, K = 5.34, H = 5.94, and J = 6.9; Epchtein et al. 1987) can be fitted by a highly reddened hot photosphere with a very small excess emission at K. The 12 and

TABLE 2

ABUNDANCES

Ion	Lines	P2
He$^+$	5876	$0.104^{+0.001}_{-0.002}$
	6678	$0.101^{+0.002}_{-0.003}$
O$^+$ $\times10^{-5}$	3727	$7.73^{+6.17}_{-2.93}$
O^{+2} $\times10^{-4}$	5007	$2.53^{+1.49}_{-0.80}$
N$^+$ $\times10^{-6}$	6584	$3.83^{+1.63}_{-0.97}$
S$^+$ $\times10^{-7}$	6716	$2.30^{+0.90}_{-0.54}$
S^{+2} $\times10^{-6}$	6312	$5.32^{+4.22}_{-2.01}$
Ne^{+2} $\times10^{-5}$	3869	$6.70^{+5.00}_{-2.44}$
Ar^{+2} $\times10^{-6}$	7136	$1.88^{+0.70}_{-0.43}$
Element	P2	Orion[a]
He	$0.104^{+0.001}_{-0.002}$	0.101
O $\times10^{-4}$	$3.30^{+2.11}_{-1.09}$	3.1
N $\times10^{-5}$	$1.64^{+0.49}_{-0.32}$	5.2
S $\times10^{-6}$	$6.77^{+5.03}_{-2.44}$	9.4
Ne $\times10^{-5}$	$8.74^{+6.96}_{-3.27}$	4.0
Ar $\times10^{-6}$	$3.52^{+1.30}_{-0.81}$	2.6

[a] Data from Osterbrock et al. (1992)

[N II] $\lambda6584$ maximum is placed between these two. Hα/[N II] and Hα/[S II] behave in opposite ways. The former is at its minimum at the ionization front (~ 9), and is 2 to 5 times larger in the surrounding region. On the other hand, Hα/[S II] is some 3 times larger at the ionization front, where it is ~ 250. Intensity profiles of [S III] $\lambda9069$ and [O III] $\lambda5007$ (not corrected for reddening) are similar to the Hα profile. Reddening does not seem to vary greatly along these vectors, but a definite statement regarding these lines is not possible given the low intensity of Hβ. Finally, RGB images which reveal the ionization structure of the whole field are presented in Figure 5. ([O III] $\lambda5007 =$ B, H$\alpha =$ G, [S III] $\lambda9069 =$ R; upper panel) and ([O III] $\lambda5007 =$ B, [N II] $\lambda6584 =$ G, [S II] $\lambda6724 =$ R; lower panel). These are continuum-subtracted images, in which any obvious traces left in the subtraction of stellar images due to differences in the PSF accross the field of view were removed for the sake of clarity. This was particularly important in the area of the starburst cluster.

Most features labelled in the Hα image have already been reported, but with a more restricted set of filters. Foremost among these structures is an "hourglass" nebula (HN) around the B1.5 supergiant Sher 25 (Brandner et al. 1997). It is dense (~ 5000 cm^{-3}) and has a large extinction (Dottori
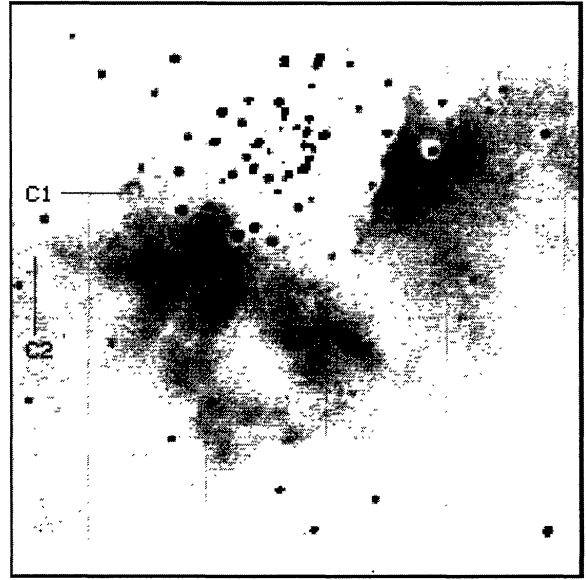

Fig. 6. [O III] $\lambda5007$/Hα ratio image of the central part of NGC 3603. C1 and C2 mark the position of "proplyd 1" and "proplyd 2" (Brandner et al. 2000), respectively. Increasing values of [O III] $\lambda5007$/Hα go from light to dark. Note the arc of highly ionized gas of 0.1 pc (3$''$) in size surrounding C1. The centre is at $\alpha = 11^{\rm h}15^{\rm m}07.4^{\rm s}$; $\delta = -61°16'19''$ (2000.0) and the field of view is 160×145 sq arcseconds. North is up, east to the left.

et al. 1999). This nebula is very prominent in the continuum-subtracted Hα and [N II] $\lambda6584$ Å frames, particularly in the latter. It is fainter in the [S III] $\lambda9069$ and [S II] $\lambda6724$ images, and barely visible in the O^{+2} continuum-subtracted image. For electron temperatures between 8000 and 10,000 K and densities in excess of 1000 cm^{-3}, N$^+$/H$^+$ $\geq$ 6×10^{-5}. Although the absence of prominent [O III] $\lambda5007$ emission is partly due to its large extinction, we may conclude that it is a mildly excited nitrogen enriched photoionized bipolar shell surrounding an evolved massive star. These are the general properties of nebulae surrounding LBV variables (e.g., Nota & Clampin 1997; Smith et al. 1997).

In a recent publication based on HST images of the region, three "proplyd-like" objects are reported (Brandner et al. 2000). These bright isolated condensations (numbers C1, C2, and C3; proplyds 1, 2, and 3 in Brandner et al. 2000) are clearly visible in all our frames. The condensations stand out with great clarity in the Hα/Hβ line ratio image: this ratio is ~ 19.5 versus ~ 14 in the surrounding environment, which implies that extinction within

TABLE 1

SPECTROSCOPIC RESULTS ($H\beta = 100$)

ID	P1		P2		P3	
	F_λ	I_λ	F_λ	I_λ	F_λ	I_λ
[O II] $\lambda3727$			24.2	113		
[Ne III] $\lambda3869$			10.3	38.5		
$H\delta$			11.4	30.8		
$H\gamma$	27.2	51.1	25.5	53.7	27.1	50.6
[O III] $\lambda4959$	151	135	185	162	136	122
[O III] $\lambda5007$	474	402	596	490	440	373
He I $\lambda5876$	40.8	14.2	51.2	14.7	42.0	14.8
[S III] $\lambda6312$			7.20	1.37		
$H\alpha$	1382	285	1841	285	1354	285
[N II] $\lambda6584$	66.0	13.5	95.1	14.5	53.6	11.1
He I $\lambda6678$	22.6	4.34	28.0	3.97	21.1	4.12
[S II] $\lambda6717$	20.1	3.77	24.1	3.32	19.1	3.64
[S II] $\lambda6731$	15.7	2.91	25.4	3.46	14.5	2.73
He I $\lambda7065$	20.7	3.19	42.4	4.63	19.0	2.98
[Ar III] $\lambda7136$	87.7	13.0	150	15.7	76.9	11.6
$F(H\beta)^a$	9.58		21.9		9.85	
$C(H\beta)$	2.12		2.51		2.10	
$I(H\beta)^b$		1.26		7.09		1.23

^{a} In 10^{-15} erg cm^{-2} s^{-1}; ^{b} in 10^{-12} erg cm^{-2} s^{-1}.

$H\alpha$ image. Textbook examples of ionization fronts are found throughout the region, some of which are marked in the [S II] $\lambda6724$ continuum subtracted image displayed in Fig. 1, which covers a 630×660 arcsec field of view. Any obvious traces left in the subtraction of stellar images due to differences in the PSF accross the field of view were removed from these images for the sake of clarity. These fronts wrap some of the densest regions of the maternal molecular cloud. Two "trunks" protrude to the SE and SW of the star cluster and open up to the south. These are $27''$ (If1) and $31''$ (If2) long (from the tip to the base where they seem to emerge), i.e., they extend for about 1 pc (for a distance of 7 kpc). It is likely that these structures were formed by a Rayleigh-Taylor instability in the dense low pressure molecular gas that is supported by the high pressure low density plasma generated by the stellar cluster. Density peaks in the molecular gas have been found immediately to the south of the base from where the trunks emerge (Melnick 1989). It would have taken $\sim 10^6/V$ yr to form a 1 pc long structure,

where V is the (mean) velocity of the perturbation in km s^{-1}. Thus, the dynamical timescale of the perturbation for a very conservative propagation velocity (1 km s^{-1}), is around half the age of the starburst cluster. Notice too that an ionization front (If3) is very close to the most recent site of star formation region (see § 3.3), and that well defined ionization fronts are found $240''$ (If4 at 8 pc) to the NE and $420''$ (If5 at 15 pc) to the SW from the central star cluster (see Figure 1).

Normalized intensity profiles of $H\alpha$, [N II] $\lambda6584$, and [SII] $\lambda6724$ accross ionization fronts If1 and If2 are depicted in Figure 4. The position angles for these cuts are $337°$ (If1) and $55°$ (If2). In both cases the origin is at the position of the $H\alpha$ maximum (close to the head of each ionization front), and positive values are inside the trunks. As can be seen, $H\alpha$ and [N II] $\lambda6584$ are strongly peaked, whereas [S II] $\lambda6724$ is far more homogeneous due to its smaller ionization potential. As expected, it is larger inside the trunk. The $H\alpha$ and [S II] $\lambda6724$ maxima are $\sim 1.4''$ distant (about 0.5 pc), while the

25 μm IRAS fluxes indicate the presence of a cool dust envelope (Epchtein et al. 1987). Although no information is available concerning the precise classification of this WR star, its color excess E_{J-H} can be accurately determined, because the intrinsic $(J - H)_0$ of all Wolf-Rayet stars is rather constant (Williams & Antonopoulou 1981). Assuming an average reddening law (Rieke & Lebofsky 1985), the total extinction towards this star is found to be $A_V \simeq 9$. Photometric distances to MR 37 can then be computed for the whole range of absolute magnitudes M_J that WR stars can have (Williams & Antonopoulou 1981; Abbott & Conti 1987). In all cases, the derived distance was significantly smaller than the distance to NGC 3603. We conclude that MR 37 is not associated to NGC 3603. This is not surprising since it is located more than 5′ away from HD 97950. The small nebulosity is not significantly different than the surrounding environment regarding Hα/Hβ and Hα/[O III], but it is markedly distinct concerning Hα/[S III], Hα/[S II], and Hα/[N II] (particularly the last two). Approximate line ratios are as follows: Hα/[N II] $\sim$ 1.6–5.9 (versus $\sim$ 30 outside) and Hα/[S II] $\sim$ 20 (versus 14 in the environment). The relative strength of the [N II] λ6584 line and weakness of the [S II] λ6724 lines imply that the nebula is nitrogen enriched and photoionized.

3.3. Broad-Band Near-Infrared Imaging

Figure 7 presents the $H - K$ versus $J - H$ diagram for sources measured in all three photometric bands. The colors have been corrected for the mean interstellar extinction towards NGC 3603, $A_V = 4.6$ assuming a standard reddening law (Rieke & Lebofsky 1985). As expected, the great majority of stars in the starburst cluster, i.e., those in the central 2.4 pc (represented by triangles), are located over a very well defined area in the two-color diagram around the locus of the photospheres of OB stars, confirming the absence of significant intracluster dust extinction. A number of sources detected in our K-magnitude-limited survey was also measured in the UBV bands by MTT. A $B - V$ versus $V - K$ diagram for the 77 stars in common is plotted in Figure 8. In this plot, most stars lie along the standard reddening vector (broken line), confirming that the interstellar and intracluster reddening law towards NGC 3603 is "normal", i.e., it resembles the mean Galactic extiction law from 0.33 to 2.5 μm. Those stars which lie significantly above the reddening vector have excess emission at $\lambda > 2$ μm.
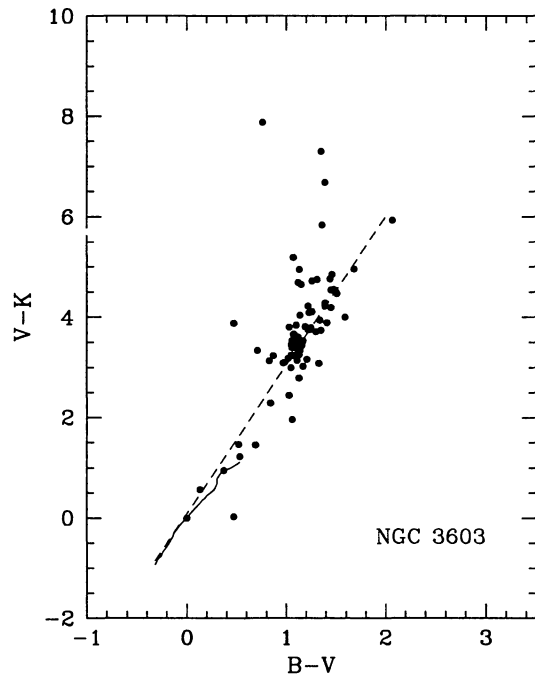

Fig. 8. $B - V$ versus $V - K$ diagram for 77 stars measured by MTT and in this work. The continuous line represents the main sequence and the broken line the Galactic mean reddening vector.

In order to get a glimpse of the effects that the huge stellar winds and UV stellar radiation from HD 97950 exert on the surrounding dense gas and dust, and in particular on recent star formation processes, we will concentrate on the sample of bright near-infrared sources which show significant excess emission at $\lambda > 2.0$ μm which we interpret as evidence of extreme youth.

Table 3 lists 50 sources with K-band excess emisssion as determined from their position in the $H - K$ versus $J - H$ diagram. We define a star to have K-band excess emisssion when its $H - K$ color index exceeds by at least 0.4 the value expected for a reddened (by any amount of A_V) OB star with the same $J - H$; that is, when it is located 0.4 magnitudes (more than twice the largest estimated error of our photometry) to the right of the reddening vector in the $H - K$ versus $J - H$ diagram (Fig. 7). The $H - K$ versus K diagram is particularly useful for studying sources fainter than our limiting magnitude in J, but red enough to have reliable H and K colors. It is important to note that due to the relatively bright limit of our survey, all stars in our diagrams that are associated with NGC 3603 have spectral types ear-

TAPIA ET AL.

TABLE 3

INFRARED-EXCESS SOURCES

R.A. (2000)	Dec.	J	H	K	Notes[a]
(h m s)	(° ′ ″)				
Irs 9 cluster					
11 15 11.4	−61 16 45	12.69	10.67	8.59	H, Irs 9, MTT 122, †
11 15 10.7	−61 16 41	13.68	13.23	11.79	
11 15 11.6	−61 16 44		14.54	13.57	
11 15 11.8	−61 16 41	14.73	13.87	12.68	
11 15 11.0	−61 16 45	15.56	14.17	11.23	H
11 15 10.0	−61 16 45	14.30	13.50	12.63	
11 15 10.3	−61 16 37	14.34	14.11	13.25	
11 15 11.1	−61 16 49		14.98	13.70	
11 15 10.3	−61 16 48	14.85	14.59	13.59	
11 15 11.0	−61 16 40		16.28	14.20	
11 15 12.4	−61 16 55		15.79	13.69	
11 15 09.3	−61 16 51	14.13	12.77	11.48	If3, G, Irs 2
11 15 05.3	−61 16 38	14.20	14.14	12.38	F
11 15 07.1	−61 16 33	14.80	14.83	13.66	
11 15 07.7	−61 16 55			8.02	MTT 58, †
Starburst cluster					
11 15 05.6	−61 15 47	12.37	10.02	8.58	MTT 120, ‡
11 15 08.2	−61 15 41	11.66	11.52	9.81	MTT 44
11 15 05.3	−61 15 16	13.93	12.62	11.28	
11 15 07.8	−61 15 35	10.50	10.47	9.56	MTT 93
11 15 04.6	−61 15 11	13.14	12.09	10.77	
11 15 07.5	−61 15 33	12.70	12.06	11.08	
11 15 08.8	−61 15 42	12.12	11.80	10.94	MTT 73
11 15 07.2	−61 16 10	13.80	13.80	12.70	
11 15 08.9	−61 15 46	12.12	12.08	10.94	MTT 29
11 15 06.9	−61 15 32	11.37	11.66	10.64	MTT 92
11 15 09.6	−61 15 42	13.93	13.46	12.63	
11 15 06.9	−61 15 42	11.02	10.24	9.22	
11 15 06.4	−61 15 41	13.58	12.59	11.25	
11 15 03.6	−61 15 46	12.02	11.28	10.13	If2, E, MTT 64
11 15 02.9	−61 15 49		12.01	10.51	If2, E, OH, H_2O
11 15 03.2	−61 15 45	12.71	12.14	10.91	If2, E
South of If 2					
11 15 02.2	−61 16 42	14.34	13.91	12.39	D
11 15 02.5	−61 16 01	13.74	13.91	12.83	Irs 1, E
11 15 00.6	−61 15 52		14.09	12.89	
11 15 03.0	−61 16 16	14.44	13.49	12.15	
11 15 04.6	−61 17 23	14.30	13.98	12.36	

TABLE 3 (CONTINUED)

R.A.	(2000)	Dec.	J	H	K	Notes[a]
(h m s)		(° ′ ″)				
Close to CO peak						
11 15 14.5		−61 17 35	14.74	14.45	13.53	J
11 15 14.0		−61 17 30	14.81	14.54	13.55	J, H_2O
11 15 14.2		−61 17 24	14.56	14.31	13.16	J, H_2O
SE regions						
11 15 15.3		−61 16 23	14.28	13.36	12.42	
11 15 17.8		−61 16 51	13.85	12.96	11.67	K
11 15 17.0		−61 16 29	13.67	12.91	11.72	
11 15 17.1		−61 16 18	13.50	13.35	12.67	
11 15 12.6		−61 16 20	13.75	13.13	12.14	
11 15 14.0		−61 16 34	14.14	13.77	12.92	
11 15 12.4		−61 15 57	13.62	13.07	12.13	
11 15 10.1		−61 16 12	13.36	13.33	11.45	If1, I, H_2O
11 15 10.4		−61 16 13	12.74	12.12	11.61	If1, I, H_2O
Proplyds						
11 15 13.1		−61 15 52	14.36	13.29	12.57	C1
11 15 16.3		−61 16 06	14.13	13.39	12.00	C2

[a]Notes: MTT: Stars from Melnick et al. (1989); Irs: Infrared sources from Frogel et al. (1977); D to K: 3.4 cm emission peaks from DePree et al. (1999); C1, C2: "Proplyds" from Brandner et al. (2000); If1, If2, If3: Ionization fronts (Fig. 1); CO emission peak from Melnick (1989); H_2O, OH: H_2O, and OH masers from Caswell et al. (1989) and Caswell (1998); †: Photometry from Roth et al. (1987) with flux from nearby stars subtracted; ‡: Photometry taken on 10 May 1988 with the ESO 1.0 m telescope at La Silla with a 5″ aperture.

TABLE 4

EVOLVED STARS IN NGC 3603

ID	R.A.	(2000)	Dec.	Spectral Type	M_v	Mk	Refs.[a]	Ident.
	(h m s)		(° ′ ″)					
Irs 9 cluster								
MTT 12	11 15 09.9		−61 15 31	O9.5Iab	−6.3		1	Sher 23
MTT 13	11 15 07.8		−61 15 17	B1.5Iab	−7.2		1	Sher 25
MTT 14	11 15 08.8		−61 16 00	O6If	−6.5		1	Sher 18
HD 97950AB	11 15 07.4		−61 15 38	2xWN6(+O?)	−7.8		1	
HD 97950C	11 15 07.7		−61 15 38	WN6(+O?)	−7.3		1	
Irs 4	11 15 03.7		−61 14 22	MIb		−8.7	2	
Irs 5	11 14 51.3		−61 13 51	MIb		−10.2	2	
Irs 6	11 15 26.2		−61 13 41	KIa		−9.1	2	
Irs 15	11 15 25.2		−61 14 50	KIab		−9.8	2	
Irs 16	11 15 16.7		−61 15 02	MIb		−7.9	3	

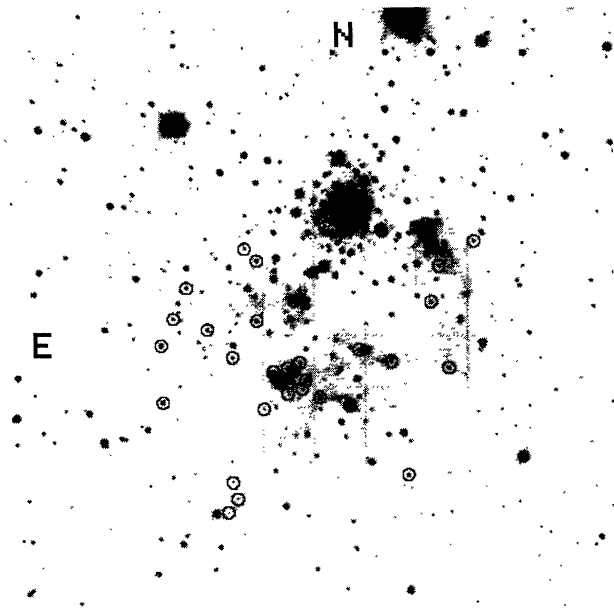[a]References: (1) Moffat et al. (1994); (2) Frogel et al. (1977), (3) Tapia (1981b).

Fig. 9. K-band mosaic marking the location of the young OB stars with near-IR excess emission. The centre is at $11^h\ 15^m\ 08.6^s$, $-61°\ 16'\ 21''$ (2000) The field of view is 245×245 sq arcseconds.

lier than B6. Thus, our near-infrared-excess sample represents the population of the youngest OB-type stars in NGC 3603. For the sake of completeness, we included in Table 3 the infrared objects located at the position of condensations C1 and C2 ("proplyds" 1 and 2 in Brandner et al. 2000), though only one shows significant near-IR excess emission.

The youngest OB stars —those with near-IR excess— in NGC 3603 are marked on the K-band mosaic shown in Figure 9. The distribution of these stars is schematically illustrated in Figure 10, where we also indicate the optical boundaries of the starburst cluster (MTT), the positions of the mid-IR (FPA), CO(1–0) and radio continuum emission (Melnick 1989; DePree et al. 1999) peaks, as well as the location of the H$_2$O and OH masers (Caswell et al. 1989; Caswell 1998).

Several important features are derived from this diagram. First, none of the infrared-excess sources is located north of the HD 93950. As pointed out by Tapia (1981a), Persi et al. (1985) and MMT, all late-type supergiants (FPA), presumably associated with a previous generation of stars in the same molecular cloud, are located to the north of the present starburst cluster (see Table 4).

Second, the majority of the youngest OB stars (80%) are clustered or associated to other signposts of recent star formation, namely, ionization fronts

(see § 3.2) and molecular gas density maxima. Furthermore, each of the hottest young OB stars has its own H II region detected in the radio continuum.

The presence of 13 young OB stars with near-IR excess (26% of our sample) distributed across the central region of the starburst cluster supports previous claims (MTT, Eisenhauer et al. 1998; Brandl et al. 1999) that the "burst" that formed the very massive cluster in NGC 3603 was **not** short-lived. The evolved massive stars at the centre of HD 97950 in their WN stage (Moffat et al. 1994), and the O-B1 supergiants in their close vicinity (all listed in Table 4), have ages above 2 million years. These cohabit with stars which appear to be much younger, including the population of low-mass pre-main sequence stars observed by Brandl et al. (1999) with ages between 0.3 and 1 million years and the young B stars reported in this paper. Thus, we consider that there is enough evidence to conclude that star formation in the core of NGC 3603 has proceeded for some 3×10^6 years and that these processes have produced, in a continuous manner, both massive and low-mass stars.

Star MTT120 is located midway between the core of HD 97950 and the ionization front If2. It stands out as the only star with strong Hα emission on our narrow-band images. It displays a large near-IR excess with $JHKL$ colors ($K - L = 1.95$), similar to star MTT122 = Irs 9. Their luminosities and colors suggest that both are very young B2-B4 type stars. consistent with the fact that neither shows a radio H II region associated and both diplay large near-IR excess emission.

The most outstanding nebulous regions in NGC 3603 (see § 3.2) —the tips of ionization fronts If1, If2 and If3— provide fascinating laboratories of active star formation induced by the interaction of a huge amount of stellar UV photons and powerful stellar winds, in this case emerging from the more than 50 WR-O-B0 stars in HD 97950, with the contiguous molecular cloud. In regions where there are considerable density enhancements we find the formation of impressive ionization fronts. As is evident from Figure 9, several young OB stars with infrared excesses included in our sample are located precisely at the heads of the elongated ionization fronts (see notes in Table 3) and all are optically very faint ($V > 20$). These represent nice examples of stars formed in these extreme conditions. As expected, stars at the tips If2 and If1 of the elephant trunks have water masers in their vicinity (Caswell et al. 1989), as is illustrated in Figure 10. The extended arc-like emission, seen predominantly in the
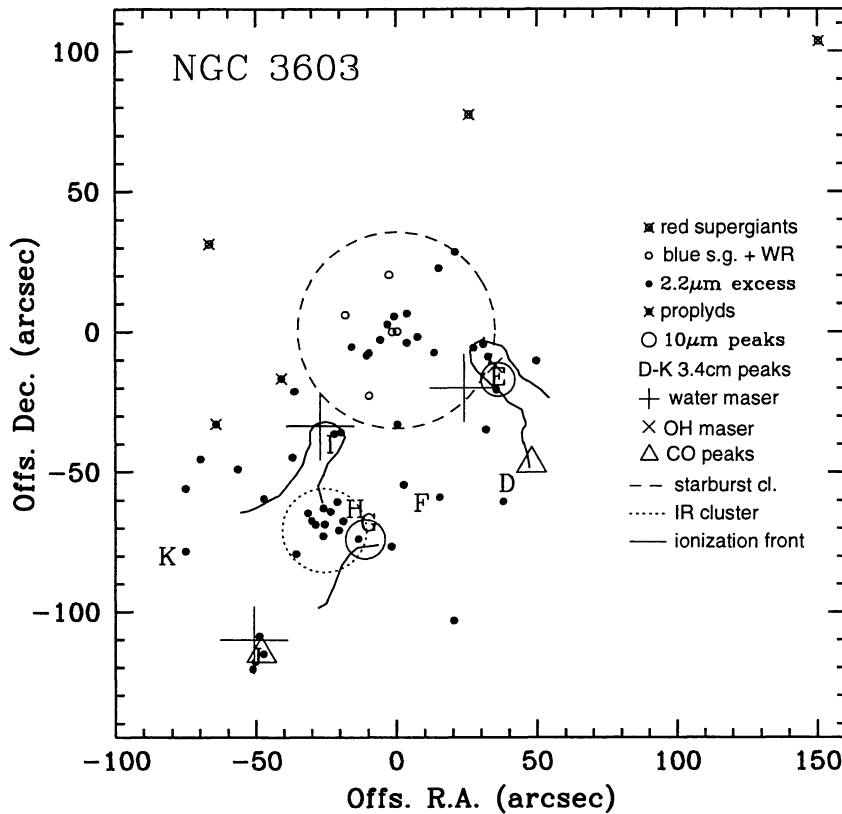
Fig. 10. Schematic representation of the distribution of the young OB stars with near-IR excess emission in NGC 3603 in relation to the boundaries of the starburst cluster, the Irs 9 embedded cluster, the ionization fronts, radio-continuum ionized-gas emission, water vapour and OH maser sources as listed in Table 3. The origin is at $11^h\ 15^m\ 11.4^s$, $-61°\ 16'\ 45''$ (2000).

K-band at these positions (see Fig. 9), was found to be dominated by molecular hydrogen emission at 2.12 μm (A. Moneti and M. Tapia, unpublished). The ionization front If2 marks the site of an active region. Three young OB stars with infrared excesses are located within a few arcseconds of the head of the trunk. The extended mid-IR emission (FPA), OH and water vapour masers (Caswell 1998; Caswell et al. 1989), as well as a radio continuum peak (E; DePree et al. 1999), all point to a rather luminous set of stars being formed in the last $\sim 10^5$ years. A quite similar scenario applies to the ionization front If1 which, with the exception of the OH maser source, shares the same characteristics with If2. It may be possible, though, that a few of the point-like sources with near-IR excesss are nebulous emission knots (probably shocked cloudlets emitting mostly in H_2), but with the available resolution this hypothesis cannot be confirmed. A few other IR-excess stars are

hot enough to ionize patches of nearby gas, as they are also seen associated with isolated 3.4 cm peaks. This is the case of radio peaks D and K (Table 3). In the latter, we also find a compact nebulous $H\alpha$ and [N II] emission knot.

Near the densest part of the molecular cloud, as mapped in the $^{12}CO(1-0)$ line by Melnick (1989), we found three very red IR-excess sources. Their position in the two-color diagram suggests that they are not very deep in the cloud. At least one of these ionizes the radio H II region J (Table 3), and has an H_2O maser source (Caswell et al. 1989) associated to it. This appears to be the active centre of massive star formation in NGC 3603 which is most distant from the starburst cluster HD 97950.

Kinematically, DePree et al. (1999) found only one of the radio H II regions to be expanding. Their data on source F is consistent with it to be an expanding shell of ionized gas. No point-like near-IR
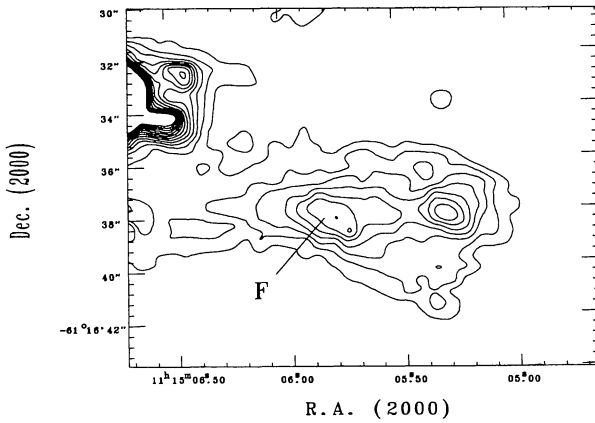
Fig. 11. K-band countour plot of the region around the position of the expanding shell F (DePree et al. (1999). The star $0.5''$ to the west of F is an infrared-excess B star (Table 3).

source is seen at this position, but rather a nebulous object elongated towards the west, pointing directly towards one of our young stellar objects (see notes in Table 3). This is seen on the K-band contour plot presented in Figure 11. The JHK colors of this object do not differ significantly from its neighbouring near-IR excess OB star.

Since its discovery by FPA, Irs 9 (star MTT 122) has been considered the most peculiar young stellar object in NGC 3603. Its near-IR colors show large infrared excess (Table 3; $K - L = 2.3$; $K - M = 3.4$: Persi et al. 1985; Roth et al. 1987). In early low resolution maps (Roth et al. 1987) it appeared extended. Its 2.0–2.5 μm spectrum is featureless (Persi et al. 1985), which is consistent with it not being associated with a radio continuum peak and implies a spectral type later than B1. The near-IR images reveal the presence of a cluster of at least 16 red stars within a $15''$ radius. What makes this cluster very peculiar is that at least 12 of them display considerable near-IR excess emission at $K > 2.0$ μm (Table 3). The amount of excess IR emission, and probably intracluster extinction, is variable from star to star. Figure 12 shows the $H - K$ versus K diagram for the stars in this very young embedded cluster. The sample of young OB stars outside HD 97950 is also included in this figure for comparison purposes. The intrinsically most luminous star of the cluster is located some $13''$ from its apparent centre, at the position of Irs 2 and the radio continuum

peak G. It is located at the edge of the ionization front If3 (Fig. 10). Its observed infrared luminosity ($> 10^5$ $L_\odot$, from 1 to 20 μm; Table 3 and FPA) is consistent with the number of UV photons required to power the radio H II region, indicating that this is an O5 – O6 star. Thus, it is the most massive of the "new generation" of stars in NGC 3603. Given its extreme youth, it is of prime importance to study the less massive stellar population of Irs 9, if already formed. The appearence of the Irs 9 cluster on the VLT color image published by Brandl et al. (1999) is inconclusive in this regard.

4. CONCLUSIONS

The combined analysis of the calibrated optical CCD narrow-band images, together with the broadband JHK imaging photometry of a large area in NGC 3603 covering the starburst cluster and H II region yields the following conclusions:
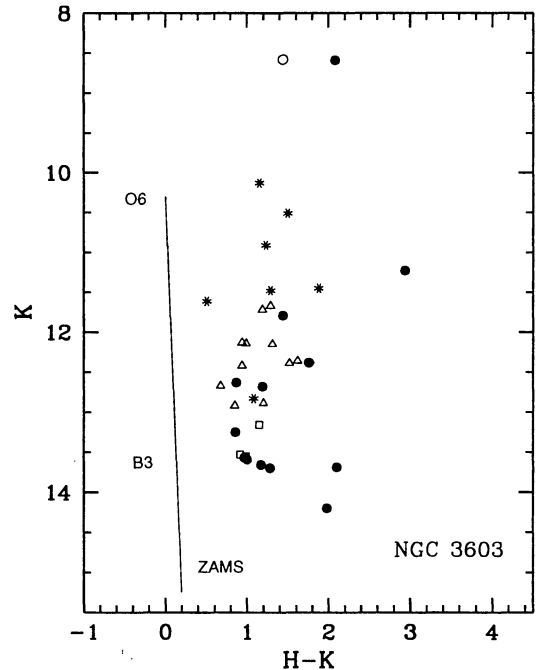

Fig. 12. $H - K$ versus K diagram for all stars with observed near-infrared excess emission outside HD 97950. Filled circles are sources in the embedded Irs 9 cluster, the open circle is MTT120, asterisks are sources associated with the heads of the ionization fronts, open squares are sources in the vicinity of the CO emission peak and open triangles are the rest of the sample. The continuous line represents the upper part of the zero age main sequence at the distance of 7.2 kpc and reddened by $E_{H-K} = 0.22$.

1. There is ample evidence that continuous star formation has occurred in the NGC 3603 molecular cloud for the last three to six million years. The first generation of massive stars is now represented by a loose concentration of a few luminous red (K and M) supergiants, all seen to the north of HD 97950. A few density enhancements of the destroyed molecular cloud are seen in their periphery. A subsequent giant burst of massive star formation resulted in the luminous optical cluster HD 97950 which powers most of the massive H II region. The starburst cluster contains more than 50 O-B0 main sequence stars as well as several evolved massive stars in their blue supergiant and Wolf-Rayet phases.

2. Further to the south, a number of massive young stellar objects, distinctive for their large near-infrared excess emission are found associated with impressive ionization fronts interacting with the rest of the molecular cloud or with thermal radio continuum and CO line emission peaks. This population includes a well defined embedded cluster which consists of at least 12 young massive O-B5 stars within a radius of 15″ (0.5 pc). The most conspicuous members of this infrared cluster are known as Irs 1 and Irs 9 (early O and B2-5 type stars, respectively). Other infrared-excess sources, such as those located on the heads of the protruding trunks and near the CO emission maximum have associated water vapour masers, confirming their extreme youth. Undoubtedly, both massive and low-mass stars continue to form in NGC 3603 till now.

3. Continuum-subtracted CCD images in the atomic lines Hα, Hβ, [N II] λ6584, [O III] λ5007, [S II] λ6724, and [S III] λ9069 were used to derive the morphological structure and distribution of the ionized species. Of particular interest are the ionization fronts around the tips of the dense trunks. A highly ionized arc of size 0.1 pc around a "proplyd-like" object is discovered. Spectroscopic observations were the basis for new abundance determinations of the nebula.

4. A number of peculiar infrared sources associated with small optical nebulosities and thermal radio continuum emission peaks are also discussed in the light of our new measurements. One of the most conspicuous is an elongated and expanding ionized gas structure (radio continuum source F) associated with a young B-type star with infrared excess in the southern part of NGC 3603.

5. The presence and characteristics of an emission-line bubble powered by the stellar wind of a Wolf-Rayet located some 5′ away from HD 97950 and apparently unrelated to NGC 3603 is reported.

Many characteristics of the NGC 3603 complex are common to 30 Doradus in the Large Magellanic Cloud. Besides the similar stellar population of their central starburst clusters and the associated expanding H II regions, we now corroborate that processes that triggered subsequent generation of stars in the outskirts of the massive clusters are similar in both regions, as a confrontation of the present results with those by Rubio et al. (1998) and Walborn et al. (1999) for 30 Doradus clearly tell us.

REFERENCES

Abbott, D. C., & Conti, P. S. 1987, ARA&A, 25, 113

Aller, L.H. 1984, Physics of Thermal Gaseous Nebula, (Dordrecht: Reidel)

Balick, B., Boeshaar, G. O., & Gull T. R. 1980, ApJ, 242, 584

Brandl, B., Brandner, W., Eisenhauer, F., Moffat, A. F. J., Palla, F., & Zinnecker, H. 1999, A&A, 352, L59

Brandner, W., Chu, Y.-H., Eisenhauer, F., Grebel, E. K., & Points, S. D. 1997, ApJ, 475, L45

Brandner, W., Grebel, E. K., Chu, Y.-H., Dottori, H., Brandl, B., Richling, S., Yorke, H. W., Points, S. D., & Zinnecker, H. 2000, AJ, 119, 292

Caswell, J. L. 1998, MNRAS, 297, 215

Caswell, J. L., Batchelor, R. A., Foster, J. R., & Wellington, K. J. 1989, Australian J. Phys. 42, 31

De Pree, C. G., Nysewander, M. C., & Goss, W. M. 1999, AJ, 117, 2902

Dottori, H., Brandner, W., Grebel, E. K., Kunkel, M., Melnick, J., Moneti, A., & Zinnecker, H. 1999, RevMexAASC, 8, Workshop on Hot Stars in Open Clusters of the Galaxy and the Magellanic Clouds, eds. N. I. Morrell, V. S. Niemela, & R. H. Barbá, (México, D. F.: Inst. Astron., UNAM), 49

Drissen, L, Moffat, A. F. J., Walborn, N. R., & Shara, M. M. 1995, AJ, 110, 2235

Eisenhauer, F., Quirrenbach, A., Zinnecker, H., & Genzel, R. 1988. ApJ, 498, 278

Epchtein, N, Le Bertre, T., Lépine, J. R. D., Marques de Santos, P, Matsuura, O. T., & Picazzio, E. 1987, A&AS, 71, 39

Frogel, J. A., Persson, E, & Aaronson, M. 1977 ApJ, 213, 723 (FPA)

Goss, W. N., & Radhakrishnan, V. 1969, Ap. Lett., 4, 199

Henize, K. G. 1976, ApJS, 30, 491

Hofmann, K.-H., Seggewiss, W., & Weigelt, G. 1995, A&A, 300, 403

Jones, T. J., Ashley, M., Hyland, A. R., Ruelas-Mayorga, A. 1981, MNRAS, 197, 413

Kingsburgh, R. L., & Barlow, M. J. 1994, MNRAS, 271, 257

Lacy, J. H., Beck, S. C., & Geball, T. R. 1982, ApJ, 255, 510

Melnick, J. 1989, The ESO Messenger, No. 57, p4

Melnick, J., Tapia, M., & Terlevich, R. 1989, A&A, 213, 89 (MTT)

Moffat, A. F. J., Drissen, L., & Shara, M. M. 1994, ApJ, 436, 183

Nota, A., & Clampin, M. 1997, in ASP Conf. Ser. Vol. 120, Luminous Blue Variables: Massive Stars in Transition, eds. S. Nota & H. J. G. L. M. Lamers (San Francisco: ASP), 303

Osterbrock, D. E., Tran, H. D., & Veilleux, S. 1992, ApJ, 389, 305

Persi, P., Tapia, M, Roth, M., & Ferrari-Toniolo, M. 1985, A&A, 144, 275

Persson, S. E., West, S. C., Carr, D. M., Sivaramakrishnan, A., & Murphy, D. C. 1992, PASP, 104, 204

Retallack, D. S., & Goss, W. M. 1980, MNRAS, 193, 261

Rieke, G. H., & Lebofsky, M. J. 1985, ApJ, 288, 618

Roberts, M. 1962, AJ, 67, 79

Roth, M., Tapia, M, Ruiz, M. T., Persi, P., & Ferrari-Toniolo, M. 1987, in IAU Symp. 115, Star Forming Regions, eds. M. Peimbert & J. Jugaku (Dordrecht: Reidel). 182

Rubio, M., Barbá, R. H., Walborn, N. R., Probst, R. G., García, J., & Roth, M. 1998, AJ, 116, 1708

Seaton, M. J. 1979, MNRAS, 187, 73P

Smith, L. J. 1968, MNRAS, 138, 109

Smith, L. J., Stroud, M. P., Esteban, C., & Vílchez, J. 1997, MNRAS, 290, 265

Stetson, P. B. 1987, PASP, 99, 191

Tapia, M., 1981a, Ph.D. thesis, University of Edinburgh
_____. 1981b, MNRAS, 197, 949

te Lintel Hekkert, P., Caswell, J. L., Habing, H. J., Haynes, R. F., & Norris, R. P. 1991, A&AS, 90, 327

Walborn, N. R., Barbá, R. H., Brandner, W., Grebel, E. K., & Probst, R. G. 1999, AJ, 117, 225

Williams, P. M., & Antonopoulou, E. 1981, MNRAS, 196, 915

Joaquín Bohigas, Brenda Pérez, and Mauricio Tapia: Instituto de Astronomía, UNAM, Apartado Postal 877, 22830 Ensenada, B. C., México (jbb,brenda,mt@astrosen.unam.mx).

Miguel Roth: Las Campanas Observatory, Carnegie Institution of Washington, Casilla 601, La Serena, Chile (miguel@lco.cl).

María Teresa Ruiz: Departamento de Astronomía, Universidad de Chile, Casilla 36-D, Santiago, Chile (mtruiz@das.uchile.cl).